Catena 141 (2016) 39–45

Contents lists available at ScienceDirect

Catena

journal homepage: www.elsevier.com/locate/catena

A novel fluorescent tracer for real-time tracing of clay transport over soil surfaces

Robert A. Hardy [a], Jacqueline M. Pates [a], John N. Quinton [a,*], Michael P. Coogan [b]

[a] Lancaster Environment Center, Lancaster University, Bailrigg LA1 4YQ, United Kingdom
[b] Chemistry Department, Lancaster University, Bailrigg LA1 4YQ, United Kingdom

ARTICLE INFO

Article history:
Received 4 November 2015
Received in revised form 11 February 2016
Accepted 12 February 2016
Available online xxxx

Keywords:
Clay
Tracing
Soil erosion
Diffuse pollution
Fluorescence
Tracer

ABSTRACT

Clay is an important vector for the transport of pollutants in the environment, including nutrients, pesticides and metals; therefore, the fate of many chemicals in soil systems is closely linked to that of clay. Understanding the mechanisms responsible for clay transport has been hampered by the lack of a suitable tracer. Producing a tracer that accurately mimics clay transport is challenging, due to the small size of the particles and their unique physical properties. Here we describe the design and synthesis of a tracer using natural clay particles as a foundation, exploiting the natural ability of clay to sorb molecules to coat the clay with a thin layer of fluorophore. Application of the tracer has been demonstrated through the collection of real-time images of the tracer moving over the surface of a soil box during a rainfall event. These images allow, for the first time, clay to be tracked spatially and temporally without need to remove soil for analysis, thus resulting in minimal experimental artefacts. Custom written software has been used to extract high resolution data describing tracer movement and extent throughout the experiment.

1. Introduction

Clay is a key component of many of the world's soils. Its ability to sorb nutrients, such as phosphorus (Sharpley et al., 1984; Sumner, 2000; Syers et al., 1971), potassium (Petrofanov, 2012), metals (Quinton and Catt, 2007) and organic pollutants (Homenauth and McBride, 1994; Sumner, 2000), and its ease of transport in flowing water makes clay an important vector for contaminant transport. Clay particles are moved by both overland flow (Quinton and Catt, 2007; Quinton et al., 2001) and by subsurface flow (McCarthy and Zachara, 1989), which may connect with rivers and lakes. Although studies have developed an empirical understanding of clay movement (Quinton and Catt, 2007; Quinton et al., 2001) and there have been attempts to model clay transport over and through soils (Jarvis et al., 1999; Jomaa et al., 2010), deriving spatial and temporal distributions of clay movement in response to rainfall has proved elusive. In this paper we describe a methodology, which, for the first time, allows the tracking of clay in time and space across a soil surface.

1.1. Tracing clay movement

Tracing clay movement has proved very challenging (Armstrong et al., 2012). One aspect of this challenge is the small size of the particles being traced. For larger particles (grains of sand size) there has been success in mixing a dye with a binding agent and then applying this mixture to the surface of the particles (Black et al., 2007). However, this technique has limitations for particles that have a diameter of a few microns, as the coating significantly alters the size and density of the particles. Therefore, for clay an alternative method of tracing is required.

This has led researchers to develop a range of techniques for tracing clay, including the use of fluorescent microspheres (Burkhardt et al., 2008; Nielsen et al., 2011), rare earth oxides (REOs), which, strictly speaking, are fine silt particles (Stevens and Quinton, 2008; Zhang et al., 2001), and the labelling of clay particles with organic molecules (Selvam et al., 2008). The majority of methods require sampling (via physical removal of material) of the soil after the experiment to determine the tracer concentration (Mabit et al., 2013; Parsons and Foster, 2011). However, it is desirable to understand how a process changes over time requiring the collection of dynamic data. Sampling interferes with detachment and transport processes, limiting the use of existing techniques for process studies. Therefore a method that does not require removal of material is required if progress is to be made in understanding the dynamics of these processes. Additionally there are significant density differences between tracers (such as microspheres and REOs) and native clay particles, which are likely to affect their transport. Therefore a clay tracer with the same physical and chemical properties as the native soil clay, and that can be manufactured easily and analysed using a non-invasive, non-destructive and in-situ analysis

* Corresponding author.
E-mail address: j.quinton@lancaster.ac.uk (J.N. Quinton).

http://dx.doi.org/10.1016/j.catena.2016.02.011

technique operating at moderate to high temporal resolution, is desirable. Some progress has been made in the nano-particle community with the creation of florescent nano-clays, however, no environmental application of the material has been reported (Diaz et al., 2013).

1.2. Fluorescence

Fluorescence detection often allows for a high signal to noise ratio permitting single molecule detection (Lakowicz, 2006). This sensitivity enables minimal fluorophore to be used in tracer production, resulting in negligible modification of the coated particle. Traditionally, fluorescence is measured on discrete samples using a fluorimeter, providing detailed spectral information. Two previous studies have captured images of fluorescent tracers using film cameras. In the first, silt-sized glass particles (44 to 2000 μm) labelled with uranium salts, which fluoresce under UV light, were monitored on a 10 m slope inclined at 5.5% (Young and Holt, 1968). Later, fluorescently-labelled pesticide granules (size unknown) were detected in soil, with each photograph imaging 0.63 m^2 (Woods et al., 1999). This work assessed how soil tillage methods affect incorporation of pesticide granules into soil; no effort was made to acquire images of the pesticide moving.

1.3. Fluorophore selection

Four principle criteria were used to select the fluorophore. It should: bind strongly to clay; fluoresce at a wavelength different to the auto-fluorescence of soil; be well characterized; and be detectable using a CMOS (Complementary Metal Oxide Sensor) detector in a digital camera. Successful binding relies on matching the fluorophore to the clay of interest; in general the fluorophore should carry the opposite charge to the clay and be lipophilic. Soil auto-fluorescence, due, in part, to the large quantity of organic aromatic acids that are present (excitation maximum at 465 nm, emission maximum at 517 nm) (Milori et al., 2002; Rinnan and Rinnan, 2007), can result in high background fluorescence and therefore interfere with detection of the tracer. Therefore to reduce the impact of natural fluorescence a fluorophore that excites between 520 and 600 nm was desired. Having a well characterized fluorophore allows more rapid progress to be made as its chemical properties are already well described. Finally, we wanted to use a CMOS detector array, commonly found in consumer grade cameras, as they acquire images within the visible range (400–700 nm). A fluorophore that fluoresces in this range was therefore required.

Rhodamine B was selected as the fluorophore, because: it binds to clay, e.g. Rhodamine B has been shown to bond organically-modified montmorillonite (Diaz et al., 2013), and sodium montmorillonite has been shown to be a successful remediation method for water contaminated with Rhodamine B (Selvam et al., 2008); it typically has an excitation maximum around 570 nm and emission maxima of around 590 nm (Beija et al., 2009), avoiding the most intense soil auto-florescence; and it fluoresces within the range detectable by a CMOS detector. Many derivatives have been synthesized, which could allow fine tuning of the clay tracer's fluorescent properties (Beija et al., 2009), and it is commercially available and inexpensive.

2. Materials and methods

Here we describe the materials and methods used to produce the clay-sized fluorescent tracer, tests of its stability and its application to a laboratory scale erosion experiment.

The instruments used were an Agilent Technologies Cary Eclipse fluorescence spectrometer and an Agilent Technologies Cary 60 UV/vis absorbance spectrophotometer. Disposable plastic cuvettes were used throughout (Fisher Scientific). The water used was deionized water, unless otherwise specified, and Rhodamine refers to Rhodamine B from Acros Organics (132311000).

2.1. Tracer production

The tracer was produced by sorbing Rhodamine onto the surface of clay particles. Twelve grammes (69904 ALDRICH) was ground to a fine powder, and sonicated for 30 min in water. Rhodamine (0.2 g) was added and the volume made up to 1 L. The mixture was sonicated for a further 45 min, stirred for 2 h, then allowed to settle. The supernatant was clear and colourless, and a vivid red-purple powder was visible at the bottom of the beaker. Excess supernatant was decanted off and the powder collected using vacuum filtration through two Whatman #5 filters. The filtrate was clear and colourless to the eye. The tracer was then thoroughly rinsed using a 50:50 mixture of saturated NaCl and ethanol and then repeatedly with water. The resulting tracer was dried at room temperature in a desiccator and protected from light. If required, the tracer was gently disaggregated by hand before use.

2.2. Tracer stability

Stability tests were carried out to ensure the tracer would not degrade over the duration of the trial (less than 24 h). One gramme of tracer (equivalent to 16.7 mg Rhodamine) was placed into 100 mL of solvent (either High Ionic Activity Solution (HIAS) or distilled water), and stirred to mix. The HIAS was prepared by combining 25 g NaCl, 4.1 g Na_2SO_4, 0.7 g KCl, 11.2 g $MgCl_2 \cdot 6H_2O$ and 2.3 g $CaCl_2 \cdot 6H_2O$ with deionized water to give a final volume of 1 L (Sverdrup et al., 1942). The aim was to produce a simulated natural water of high ionic activity with respect to the major elements. The concentrations used in this solution are extreme compared to those normally found in terrestrial waters; if the tracer is stable under these conditions, we assume that it will be stable in the vast majority of soil environments.

After a period of time (>40 h), during which the tracer was allowed to settle, 3 mL of the supernate was placed in a plastic cuvette to assess desorption of Rhodamine from the tracer, using UV/vis absorbance spectrophotometry and fluorescence spectrometry. No attempt to separate the tracer from the water was made, as any particles remaining in suspension were too fine to remove by filtration.

To make calibration standards, first a stock solution was prepared by dissolving 18.2 mg Rhodamine in 100 mL deionized water. Standards for UV/vis spectrophotometry and fluorescence spectrometry were prepared by diluting the stock 1:250 for fluorescence measurements and 1:125 for UV/vis measurements, using either HIAS or deionized water. Thus, the UV/vis standards contained 0.144 mg Rhodamine per 100 mL, and the fluorescence standards contained 0.072 mg Rhodamine per 100 mL. These are the concentrations that would be achieved had 1% or 0.5% Rhodamine dissolved off the tracer during the stability experiments.

2.3. Physical properties of tracer

A Leica confocal microscope was used to record images of clay and tracer particles. Images were taken using a 63× optical lens under oil. The size range of particles was measured using a Malvern Mastersizer 2000.

2.4. Acquiring fluorescent images

Images were acquired using a Canon 500-D DSLR camera mounted on a tripod. (See Supplementary information (SI) 1: Camera setup, for further details of the camera settings and filters). A ~75 mW, 532 nm (green) laser was used to illuminate the soil box, after passing through a rotating diffuser (SI 2: Laser lighting setup, SI: Fig. S1). Achieving uniform illumination is critical to producing accurate images (Waters, 2009). Visual and photographic assessment of the light showed an acceptable degree of uniformity (SI: Fig. S2).

2.5. Soil box

Perspex soil boxes (350 mm by 500 mm), with drainage holes in the base, were filled with 4 cm fine gravel, landscape fabric membrane, 3 cm sand and 4 cm soil (screened to 4 mm) to simulate natural infiltration conditions following Armstrong et al.'s method (Armstrong et al., 2012). The soil was a clay loam soil of the Wick 1 association from Lancaster, Lancashire, United Kingdom. A 150 × 50 × 5 mm section of soil was removed, mixed with 4 g of tracer and then replaced (Fig. 1). To bring them to near saturation, the soil boxes were immersed in water, to a depth 1 cm above the soil–sand interface, for 22 h. The box was then drained for one hour and exposed to rainfall, while set at a slope of 4%.

2.6. Rainfall

A gravity-fed rainfall simulator was used to deliver rainfall with an intensity of 42 mm h^{-1} using reverse osmosis (RO) grade water (Armstrong et al., 2012).

2.7. Runoff testing

Runoff was collected from the run-off collector (Fig. 1), with the container receiving the run-off changed every 5 min. Runoff collected from between 30 and 45 min after rainfall has commenced was bulked and vacuum filtered using two Whatman #5 filters to remove the particulates.

3. Results

3.1. Tracer stability

In order for a tracer to be useful it must remain intact for the duration of the study. The most likely route of tracer degradation is desorption of Rhodamine from the clay surface. To investigate this possibility, UV/vis absorbance and fluorescence spectrometry were used to characterize the loss of Rhodamine upon exposure to HIAS or distilled water (over 40 h).

The supernate showed virtually no absorbance of light in the UV/vis range due to solution phase Rhodamine, as demonstrated by the lack of a peak at ~560 nm (Fig. 2a and b). Fig. 2a shows a raised baseline attributed to fine, colloidal-sized particulate matter (the tracer) remaining in suspension scattering the light, a hypothesis supported by the lack of specific absorption bands. The small peak at ~590 nm is assigned to Rhodamine as no other component absorbs in that region. However the wavelength maximum does not match that of the Rhodamine standard, which suggests that the Rhodamine responsible for this peak is modified compared to the standard. An interaction between Rhodamine and montmorillonite, either through chemisorption onto the surface, or simple protonation (the montmorillonite used is pH 3), could account for this shifted wavelength. The absence of a raised baseline in HIAS (Fig. 2b) suggests that there are no tracer particles present; we propose that the high ionic strength of HIAS encourages flocculation and hence precipitation out of the clay tracer (Elimelech et al., 1995).

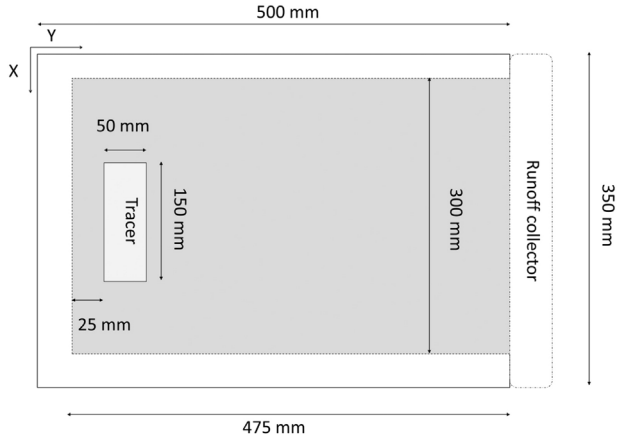

Fig. 1. Schematic of the soil box used showing starting location of tracer. The grey area is the imaged area.

Fluorescence measurements showed a peak with a maximum emission at 575 nm, attributed to dissolved Rhodamine, in the HIAS solution (Fig. 2d). In order to estimate the amount of Rhodamine lost from the tracer during the experiment, linearity between the sample and standard was assumed and the following equation used to estimate the amount of Rhodamine lost: (standard concentration / fluorescence intensity of standard) × fluorescence intensity of sample. This relationship suggests that approximately 0.022 mg Rhodamine was lost from the tracer, i.e. 0.13% of the total amount used in the experiment. A broader and flatter peak is seen in the deionized water sample (Fig. 2c), indicative of minimal desorption from the tracer. The greater desorption of Rhodamine in HIAS is probably due to the high ionic strength of the solution, whereby the HIAS ions compete with the Rhodamine for binding sites on the clay forcing the latter to desorb. However, HIAS has a much higher ionic strength than water soil mixtures, where the tracer will be deployed; therefore it is reasonable to assume that desorption will not readily occur during soil transport experiments.

3.2. Physical properties of tracer

Comparing the particle size distribution of the tracer and the clay from which the tracer was made, it was found that 55% of the tracer had a size of less than 2 μm, compared to 51% of the montmorillonite. Furthermore, the size distribution of the particles before and after treatment with Rhodamine was consistent (SI 3: Tracer size). Confocal microscope images show that the particles retain their irregular sizes and shapes (Fig. 3a and b). The Rhodamine appears to be uniformly distributed over the particle surface, without disturbing surface texture (Fig. 3c). The appearance of more rings around the clay in the phase contrast image of the tracer is consistent with the hydration of the clay during synthesis of the tracer.

3.3. Tracer movement images

The images show, for the first time, clay movement over a soil surface in real time under continuous simulated rainfall conditions (Fig. 4 and SI 4: Images). The movement of tracer across the whole soil box was recorded every 7 s from a distance of ~2 m. The sample area is 2431 × 1769 pixels (0.135 m^2), which equates to approximately 31 pixels per mm^2. As no soil was physically removed from the box during the experiment, there was no external disturbance to the system, resulting in fewer sampling artefacts. By increasing the light input (by increasing the camera aperture and moving the light source closer to the target) and sensitivity of the CMOS detector (by increasing the ISO setting), the soil box was imaged on the sub-second time scale (every 0.8 s), although increased noise was present (SI 5: Rapid imaging).

3.4. Image processing

Although it is possible to view the images without post-processing, much can be gained from doing so. Using [R] (Hijmans, 2014; Polzehl and Tabelow, 2007; R Development Core Team, 2013; Urbanek, 2013), the images were converted to false colour with noise suppressed (Fig. 4). Further details of the image processing methods can be found in SI 6: Image processing. These images were easier to analyse visually, as they show the presence of tracer in green and the absence in white. The file size of the images is approximately 100 times smaller than the original images. Images of this nature were then compressed (Cinepak

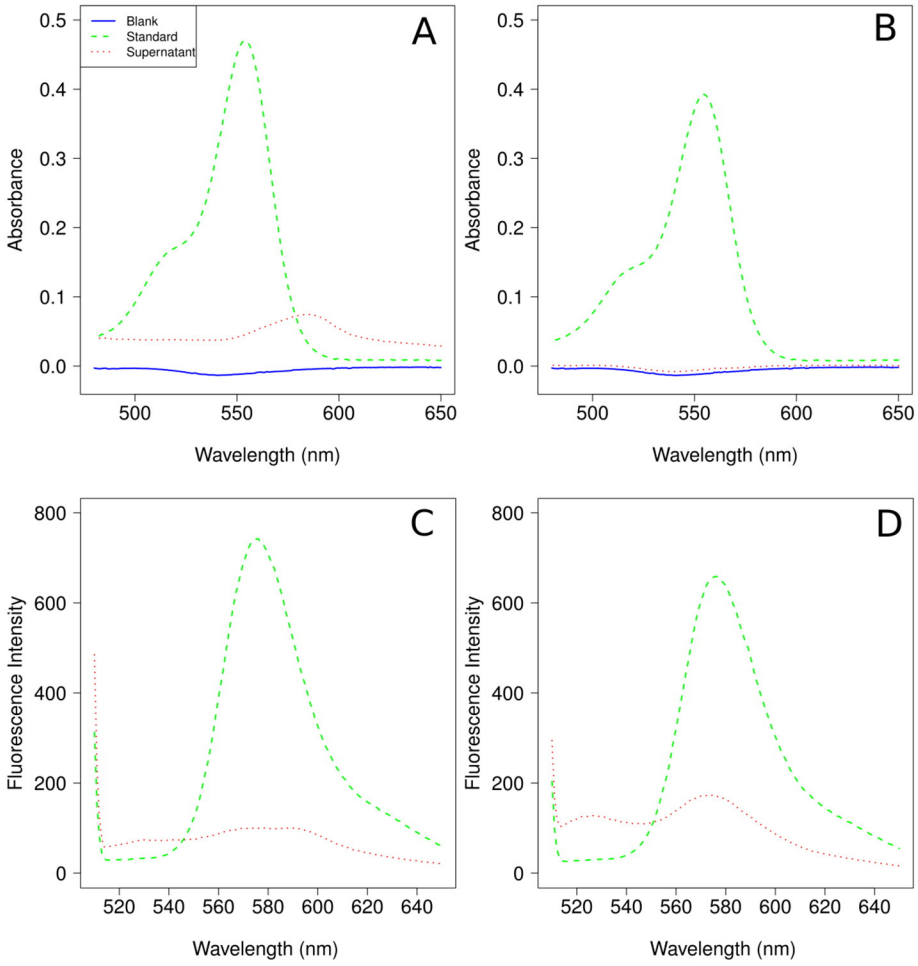

Fig. 2. UV/vis (A and B) and fluorescence spectra (C and D) of supernatant solutions. The tracer was mixed with either deionized water (A and C) or high ionic activity solution (B and D) and the supernatant separated after more than 40 h, to test for desorption of Rhodamine.

codec by Radius, quality 100) into a time-lapse video using VirtualDub (version 1.10.4) allowing the whole event to be reviewed in less than a minute.

The intensity of fluorescence from the tracer, in the solid state, is independent of the concentration of tracer. This type of behaviour is symptomatic of self-quenching, which involves the rapid exchange of energy between molecules and de-excitation via non-radiative processes, typically relaxation to the ground state through vibrational levels. Due to the close spatial proximity of the Rhodamine molecules to one another when bound to clay and the small Stokes shift (and therefore overlap of excitation and emission bands), this type of behaviour is neither unusual nor unexpected (Lakowicz, 2006). As the amount of light emitted from the tracer is not a function of the tracer concentration, the intensity of light cannot be used to quantify the amount of tracer at a given point. Nonetheless, the true-colour images shown (Fig. 4a–c) have some qualitative properties, as areas that are much more intensely coloured are likely to contain more tracer than those that are less intensely coloured.

We have confidence that interference due to autofluorescence was not a problem as we have used constant illumination and the initial

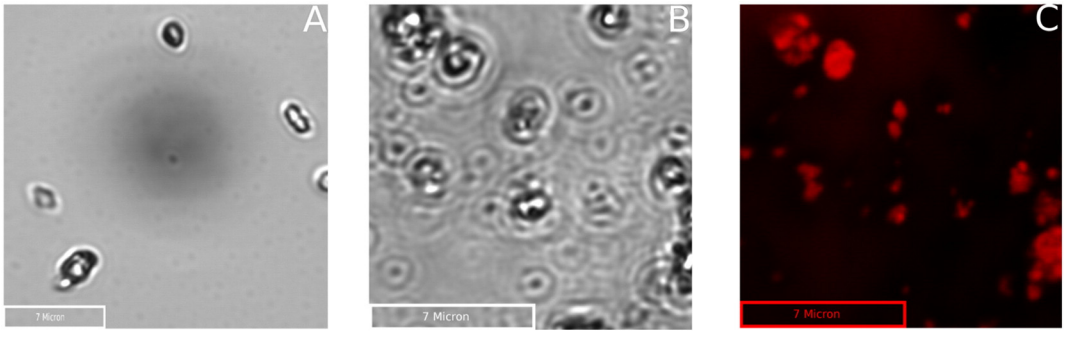

Fig. 3. Confocal micrographs of clay tracer: A) phase contrast before treatment with Rhodamine; B) phase contrast after treatment with Rhodamine; and C) false colour fluorescent after treatment with Rhodamine. Note that the clay retains its size and shape after treatment and that the fluorescence appears quite uniformly on the clays surface.

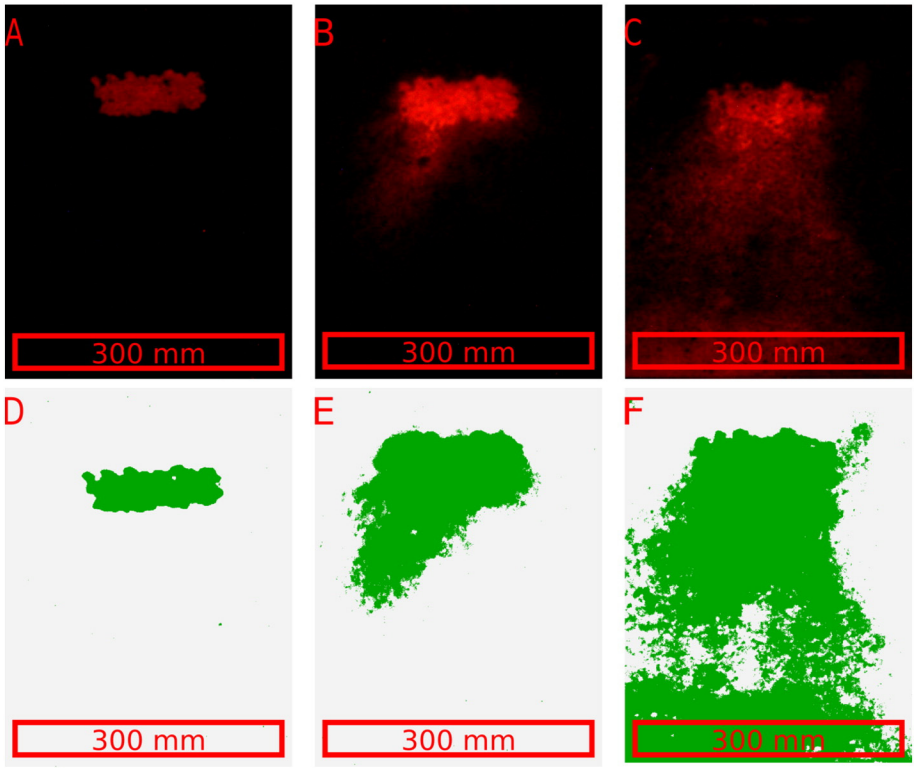

Fig. 4. Images of soil box (top of box at top of image) showing tracer location at various times. A to C are true colour images and D to F are false colour images produced using [R]. A and D were before exposure to rain, B and E are after 262 s of rain and C and F are after 2252 s. After 0 s the tracer was constrained to the area where it was applied. After 262 s the tracer had moved down the box and spread laterally, further movement and lateral spreading continued until the experiment was ended at 2252 s. Transport pathways of clay from the top of the box to the bottom can be observed together with a depositional area which formed at the bottom edge of the box.

images (Fig. 4a and d) show intense colour where the tracer was applied and virtually no colour anywhere else.

3.5. Runoff testing

In order for the tracer to be useful it must remain intact throughout the experiment, which can be evaluated by recovering the tracer afterwards. Particulate material recovered from the runoff, was dried and photographed on a black (non-fluorescent) background (Fig. S4). The colour and intensity seen in Fig. S4 are very similar to the colour and intensity seen in Fig. 4, suggesting that the tracer has remained intact throughout the experiment.

The filtrate was a reddish brown to the eye, which were attributed to fine particles, given that they are illuminated when a ~1 mW (532 nm) laser beam is passed through the suspension (an effect not seen in particle-free solutions). The filtrate was centrifuged at 15,000 rpm for 99 min, the supernatant decanted and then imaged on a non-fluorescent background, using standard image acquisition and processing parameters. No fluorescence was seen (Fig. 5), in contrast to a solution containing 2 μg/L Rhodamine, which could be

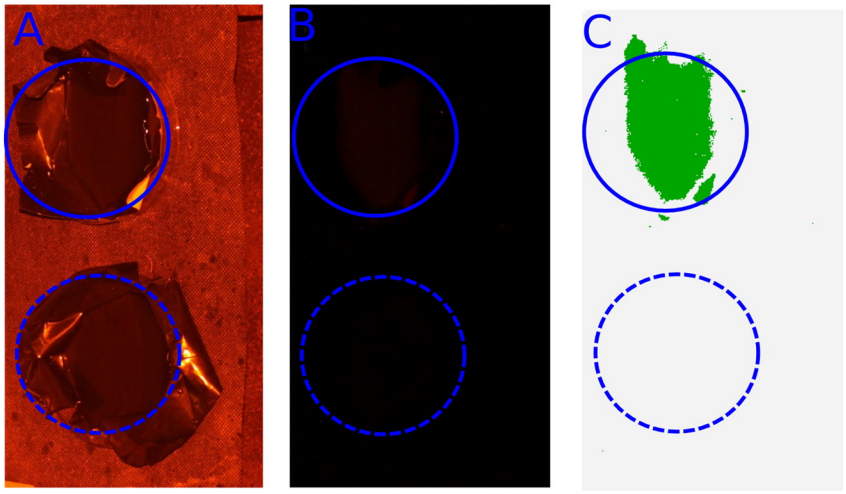

Fig. 5. Comparison of soil-box runoff in a Petri dish backed with black plastic after filtration and ultra-centrifugation with a Rhodamine standard. The solid circles show the location of the standard (2 μg/L) while the dotted circles show the filtered and ultra-centrifuged soil-box runoff. A is a true colour image captured under typical room lighting with a 570 nm long pass filter on the camera, B is a recorded using 532 nm lighting and a 570 nm filter, and C is a false colour image process using R. The standard is clearly detectable in C but not the runoff.

readily detected. We are therefore confident that the images in Fig. 4a, b, c are images of the Rhodamine-labelled clay rather than Rhodamine in solution.

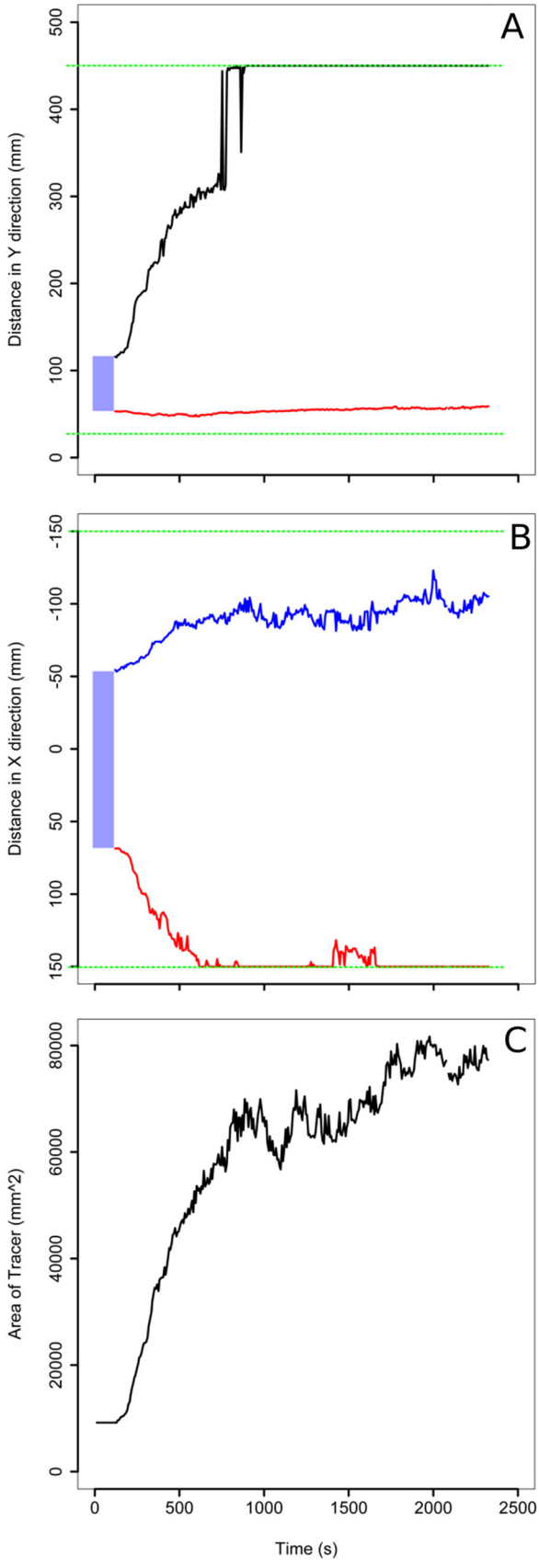

3.6. Demonstration of application

In order to demonstrate how high temporal and spatial resolution data can be used in the study of soil erosion processes, the tracer front was mapped against time (Fig. 6a). The data were extracted from 312 images using a custom written function in [R] (SI 10: Tracking tracer spread). The effect of rain-splash was analysed by looking at how the tracer front moved up and down the box (Fig. 6a), which demonstrates the dynamic nature of both the upper and lower tracer fronts. As expected the movement down the box is more rapid than that up the box. The lower tracer front moves rapidly to begin with, slows and then moves rapidly again. We attribute this behaviour to changes in soil microtopography akin to a dam bursting, allowing overland flow to connect with the bottom of the box and rapidly deliver the tracer. The spike at approximately 1000 s is attributed to an artefact in the data. Lateral spreading of the tracer was also noticed in the images so a plot correlating the width of the tracer band to time was also produced (Fig. 6b), as well as the changing tracer area over time (Fig. 6c). The development of the tracer area can viewed dynamically in the online version of the papers (Video 1).

4. Discussion

We have developed a tracing and imaging method that, for the first time, allows clay movement to be traced, with a millimetre precision in two dimensions with a time-step of approximately 1 s, under simulated rainfall conditions without the need to stop the experiment to take samples. This is a major advance over previously reported techniques. Previous work has focused on the use of exotic particles and elemental tagging in soil tracing; examples include fluorescent microspheres (Pryce, 2011), ceramic prills (Duke et al., 2000; Plante et al., 1999), plastic magnetic beads (Ventura et al., 2001) and REOs (Deasy and Quinton, 2010). These methods have been criticized as the tracers have different physical properties, such as size, shape and density, to the target soil (Zhang et al., 2003). By using natural particles as the basis for this tracer we believe that we have minimized or avoided many of these problems; physically, the tracer retains the same size and density characteristics as the native clay and aggregates in the same way as the untreated clay.

The second advantage over existing methods is the ability to capture spatial information, without the need to destructively sample the experiment, and temporal information throughout the experiment, allowing highly dynamic changes in tracer distribution to be captured. Other than work utilizing magnetic susceptibility (e.g. Armstrong et al., 2012), experimenters have largely relied on destructive sampling at the end of an experiment in order to understand surface processes. Destructive sampling has limited spatial resolution, because of the size of samples required (typically >2 cm^2), is laborious, and for many tracers requires subsequent analysis. The temporal and spatial resolutions of our tracer will allow us to gain insights into the controls on colloidal detachment and transport, and have the potential to enable the spatial testing of distributed models of size-selective erosion processes (Heng et al., 2011).

The system we have described is limited in scale to a 0.5 m × 0.4 m soil box, constrained by the field of view of the camera as well as the area that can be illuminated with the laser. Larger fields of view could be used to expand the area that can be imaged; however this would reduce the resolution of the system. Working on larger study areas will require a brighter laser for illumination and either multiple cameras

Fig. 6. The movement of the tracer over time. The imageable area is bounded by the dashed green lines and the blue box represents the original location of the tracer. A shows the movement of the tracer in direction Y (the primary direction of water flow), B shows the lateral spread of tracer in direction X (orthogonal to the primary direction of water flow), and C shows the total area that the tracer occupies. All changes are shown against time. (For interpretation of the references to colour in this figure legend, the reader is referred to the web version of this article.)

to capture multiple images, which could be stitched together in post-processing, or a super-camera with a large frame area and high density of pixels, for example the qG (Aqueti Inc.), which is 250 megapixel camera with a 50 × 24 degree field of view.

This new tracing methodology will open up new opportunities to understand clay transport and associated pollutants and nutrients, helping us to develop a better understanding of these dynamic processes. There is potential to develop the system further to provide a tracer and detection method for field-based deployment and the quantification of tracer concentrations, opening up new possibilities for understanding the fate and behaviour of sediment and contaminants in the environment.

Diagrams relating to equipment design, camera and lighting conditions, computer code, runoff testing and demonstration of application can be found in the Supporting information. Supplementary data associated with this article can be found in the online version, at doi:10.1016/j.catena.2016.02.011.

Acknowledgements

R.H. is funded by a joint U.K. Natural Environment Research Council–Analytical Chemistry Trust Fund Studentship (NE/J017795/1). Thanks to Mike James for his support with image processing and Debbie Hurst for the microscope images. More information about the underlying data in this paper is available from http://dx.doi.org/10.17635/lancaster/researchdata/65.

References

Armstrong, A., Quinton, J.N., Maher, B.A., 2012. Thermal enhancement of natural magnetism as a tool for tracing eroded soil. Earth Surf. Process. Landf. 37, 1567–1572.
Beija, M., Afonso, C.A.M., Martinho, J.M.G., 2009. Synthesis and applications of Rhodamine derivatives as fluorescent probes. Chem. Soc. Rev. 38, 2410–2433.
Black, K.S., Athey, S., Wilson, P., Evans, D., 2007. In: Balson, P.S., Collins, M.B. (Eds.), Coastal and Shelf Sediment Transport. Geological Society, Special Publications, London, pp. 73–91.
Burkhardt, M., Kasteel, R., Vanderborght, J., Vereecken, H., 2008. Field study on colloid transport using fluorescent microspheres. Eur. J. Soil Sci. 59, 82–93.
Deasy, C., Quinton, J.N., 2010. Use of rare earth oxides as tracers to identify sediment source areas for agricultural hillslopes. Solid Earth 1, 111–118.
Diaz, C.A., Xia, Y., Rubino, M., Auras, R., Jayaraman, K., Hotchkiss, J., 2013. Fluorescent Labeling and Tracking of Nanoclay 5 pp. 164–168.
Duke, M.J.M., Plante, A.F., McGill, W.B., 2000. Application of INAA in the characterisation and quantification of Dy-labeled ceramic spheres and their use as inert tracers in soil studies. J. Radioanal. Nucl. Chem. 244, 165–171.
Elimelech, M., Gregory, J., Jia, X., Williams, J.A., 1995. Particle Deposition and Aggregation: Measurement, Modelling and Simulation. Butterworth-Heinemann, Oxford, England.
Heng, B.C.P., Sander, G.C., Armstrong, A., Quinton, J.N., Chandler, J.H., Scott, C.F., 2011. Modeling the dynamics of soil erosion and size-selective sediment transport over nonuniform topography in flume-scale experiments. Water Resour. Res. 47, W02513.
Hijmans, R.J., 2014. raster: geographic data analysis and modeling. https://cran.r-project.org/web/packages/raster/index.html.
Homenauth, O.P., McBride, M.B., 1994. Adsorption of aniline on layer silicate clays and an organic soil. Soil Sci. Soc. Am. J. 58, 347–354.
Jarvis, N.J., Villholth, K.G., Ulen, B., 1999. Modelling particle mobilization and leaching in macroporous soil. Eur. J. Soil Sci. 50, 621–632.
Jomaa, S., Barry, D.A., Brovelli, A., Sander, G.C., Parlange, J.Y., Heng, B.C.P., Tromp-van Meerveld, H.J., 2010. Effect of raindrop splash and transversal width on soil erosion: laboratory flume experiments and analysis with the Hairsine–Rose model. J. Hydrol. 395, 117–132.
Lakowicz, J.R., 2006. Principles of Fluorescence Spectroscopy. Springer, New York.
Mabit, L., Meusburger, K., Fulajtar, E., Alewell, C., 2013. The usefulness of ^{137}Cs as a tracer for soil erosion assessment: A critical reply to Parsons and Foster (2011). Earth-Sci. Rev. 127, 300–307.
McCarthy, J.F., Zachara, J.M., 1989. Subsurface transport of contaminants. Mobile colloids in the subsurface environment may alter the transport of contaminants. Environ. Sci. Technol. 23, 496–502.
Milori, D., Martin-Neto, L., Bayer, C., Mielniczuk, J., Bagnato, V.S., 2002. Humification degree of soil humic acids determined by fluorescence spectroscopy. Soil Sci. 167, 739–749.
Nielsen, M.H., Styczen, M., Ernstsen, V., Petersen, C.T., Hansen, S., 2011. Distribution of bromide and microspheres along macropores in and between drain trenches. Vadose Zone J. 10, 345–353.
Parsons, A.J., Foster, I.D.L., 2011. What can we learn about soil erosion from the use of Cs-137? Earth-Sci. Rev. 108, 101–113.
Petrofanov, V.L., 2012. Role of the soil particle-size fractions in the sorption and desorption of potassium. Eurasian Soil Sci. 45, 598–611.
Plante, A.F., Duke, M.J.M., McGill, W.B., 1999. A tracer sphere detectable by neutron activation for soil aggregation and translocation studies. Soil Sci. Soc. Am. J. 63, 1284–1290.
Polzehl, J., Tabelow, K., 2007. Adaptive smoothing of digital images: the R package adimpro. J. Stat. Softw.
Pryce, O., 2011. Development of Environmental Tracers for Sediments and Phosphorus. Lancaster University (PhD thesis).
Quinton, J.N., Catt, J.A., 2007. Enrichment of heavy metals in sediment resulting from soil erosion on agricultural fields. Environ. Sci. Technol. 41, 3495–3500.
Quinton, J.N., Catt, J.A., Hess, T.M., 2001. The selective removal of phosphorus from soil: is event size important? J. Environ. Qual. 30, 538–545.
R Development Core Team, 2013. R: A Language and Environment for Statistical Computing.
Rinnan, R., Rinnan, Å., 2007. Application of near infrared reflectance (NIR) and fluorescence spectroscopy to analysis of microbiological and chemical properties of Arctic soil. Soil Biol. Biochem. 39, 1664–1673.
Selvam, P.P., Preethi, S., Basakaralingam, P., Thinakaran, N., Sivasamy, A., Sivanesan, S., 2008. Removal of rhodamine B from aqueous solution by adsorption onto sodium montmorillonite. J. Hazard. Mater. 155, 39–44.
Sharpley, A.N., Smith, S.J., Stewart, B.A., Mathers, A.C., 1984. Forms of phosphorus in soil receiving cattle feedlot waste. J. Environ. Qual. 13, 211–215.
Stevens, C.J., Quinton, J.N., 2008. Investigating source areas of eroded sediments transported in concentrated overland flow using rare earth element tracers. Catena 74, 31–36.
Sumner, M.E., 2000. Handbook of Soil Science. CRC Press, Boca Raton, Fla.
Sverdrup, H.U., Johnson, M.W., Fleming, R.H., 1942. The Oceans, Their Physics, Chemistry, and General Biology. Prentice-Hall, Inc., New York.
Syers, J.K., Evans, T.D., Williams, J.D., Murdock, J.T., 1971. Phosphate sorption parameters of representative soils from Rio Grande Do Sul, Brazil. Soil Sci. 112, 267–275.
Urbanek, S., 2013. tiff: Read and write TIFF images.
Ventura, E., Nearing, M.A., Norton, L.D., 2001. Developing a magnetic tracer to study soil erosion. Catena 43, 277–291.
Waters, J.C., 2009. Accuracy and precision in quantitative fluorescence microscopy. J. Cell Biol. 185, 1135–1148.
Woods, S., Haydock, P.P.J., Evans, K., Robinson, R.C., Dawkins, T.C.K., 1999. Use of fluorescent tracer techniques and photography to assess the efficiency of tillage incorporated granular nematicides into potato seed-beds. Soil Tillage Res. 51, 17–23.
Young, R.A., Holt, R.F., 1968. Tracing soil movement with fluorescent glass particles. Soil Sci. Soc. Am. Proc. 32, 600–602.
Zhang, X.C., Friedrich, J.M., Nearing, M.A., Norton, L.D., 2001. Potential use of rare earth oxides as tracers for soil erosion and aggregation studies. Soil Sci. Soc. Am. J. 65, 1508–1515.
Zhang, X.C., Nearing, M.A., Polyakov, V.O., Friedrich, J.M., 2003. Using rare-earth oxide tracers for studying soil erosion dynamics. Soil Sci. Soc. Am. J. 67, 279–288.